ACS Catalysis

Research Article

pubs.acs.org/acscatalysis

Mechanism and Origins of Selectivities in the Copper-Catalyzed Dearomatization-Induced *ortho* C−H Cyanation of Vinylarenes

Yang Yang[†,‡] and Peng Liu*[,‡]

[†]Department of Chemistry, Massachusetts Institute of Technology, Cambridge, Massachusetts 02139, United States

[‡]Department of Chemistry, University of Pittsburgh, Pittsburgh, Pennsylvania 15260, United States

Supporting Information

ABSTRACT: The mechanism of the copper-catalyzed regioselective *ortho* C−H cyanation of vinylarenes has been investigated using density functional theory calculations. This C−H cyanation is composed of two discrete catalytic cycles (the copper-catalyzed electrophilic cyanative dearomatization and the subsequent base-catalyzed hydrogen transposition) that furnish the *ortho* C−H cyanated arenes. The electrophilic cyanation step features a unique six-membered transition state, leading to the formation of the dearomatized intermediate with a high level of site selectivity. Such dearomatization significantly increases the reactivity of the C−H bond, thereby enabling the base-assisted C−H activation in the following steps.

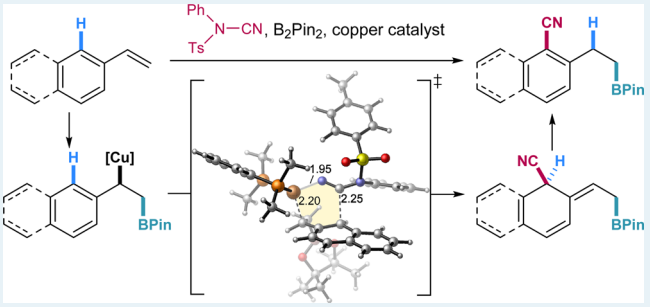

KEYWORDS: *DFT, C−H functionalization, dearomatization, cyanation, copper catalysis*

1. INTRODUCTION

Transition-metal-catalyzed C−H functionalization has become a powerful tool in the synthetic chemist's repertoire.[1,2] In particular, the recent development of chelation-assisted *ortho*-selective C−H functionalization has culminated in a range of synthetically versatile transformations.[1] However, in contrast to numerous well-developed techniques to activate C(sp^2)−H bonds *ortho* to relatively strong σ-chelating directing groups such as pyridines[1a,f] and carbonyls,[1c−e] the selective functionalization of C−H bonds *ortho* to a weakly coordinating π-ligand such as an olefin remains challenging.[3]

In this regard, Yang and Buchwald recently reported an *ortho*-selective C−H cyanation of vinylarene derivatives triggered by olefin borylation using inexpensive copper catalysts featuring a high level of site selectivity (Schemes 1 and 2).[4,5] Preliminary mechanistic studies[4] led us to postulate that this C−H cyanation process involves an unconventional copper-catalyzed electrophilic dearomatization mechanism. As shown in Scheme 1, interception of the benzylcopper intermediate **II** generated from borocupration of styrene **I** by a proper electrophile (e.g., NCTS[6] (**2**)) leads to the formation of a highly reactive dearomatized intermediate **III**, which in turn undergoes a 1,3-hydrogen transposition to furnish the *ortho* C−H functionalized product **IV**. The key step in this proposed mechanism, the catalytic dearomatization involving benzylcopper intermediates, has rarely been reported.[7] The exact mechanism of this novel transformation and the origin of the selectivity for the dearomatization intermediate are not clear. In addition, strategies utilizing dearomatization as a driving force for selective C−H functionalization of arenes remain to be developed. We envisioned that a thorough mechanistic understanding and a predictive model for the regioselectivity of the cyanation reaction could aid in the further development of this dearomatization-induced C−H functionalization strategy. Herein we report our computational study on the mechanism of this Cu-catalyzed dearomatization/C−H functionalization (Scheme 3). We revealed the factors that contribute to the high level of selectivity observed in the borocupration and the electrophilic cyanation steps. Furthermore, we provide computational evidence in support of a base-catalyzed mechanism for the hydrogen transposition event.

Scheme 1. Copper-Catalyzed Dearomatization-Induced C−H Functionalization: A New Strategy for the Selective *ortho* C(sp^2)−H Functionalization of Vinylarenes

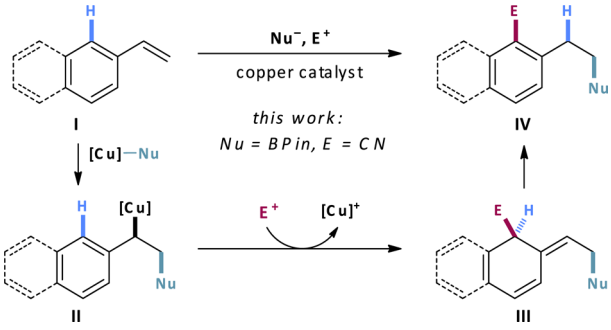

Received: March 2, 2015
Revised: April 2, 2015
Published: April 6, 2015

DOI: 10.1021/acscatal.5b00443
ACS Catal. 2015, 5, 2944−2951

Scheme 2. Distinct Regioselectivity in the Copper-Catalyzed C−H Cyanation[4]

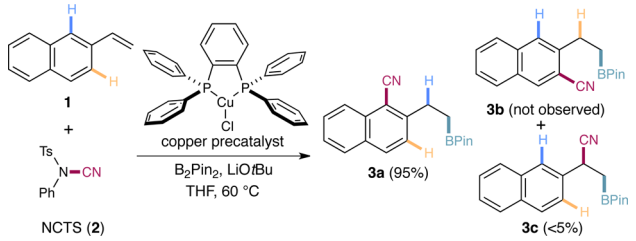

2. COMPUTATIONAL DETAILS

All calculations were performed with Gaussian 09.[8] Images of the 3D structures of molecules were generated using CYLView.[9] The geometries of all intermediates and transition states were optimized with the B3LYP[10] functional in gas phase. A mixed basis set of SDD for Cu and 6-31G(d) for other atoms were used in geometry optimizations. Single-point energy calculations were performed with the M06[11] functional and a mixed basis set of SDD for Cu and 6-311+G(d,p) for other atoms. The SMD[12] solvation model was used in M06 single point energy calculations with THF as the solvent. The reported free energies and enthalpies include zero-point energies and thermal corrections calculated at 298 K with B3LYP/SDD−6-31G(d). All energies in the energy profiles are with respect to the separate reactant **1** or **15** and the active catalyst **4**. The combination of using a GGA or hybrid GGA functional, such as BP86 and B3LYP, for geometry optimizations and a *meta* hybrid GGA functional, such as M06, for single-point calculations was used in most of the recent computational studies on transition metal-catalyzed reactions.[13] This approach has also been recommended by several recent benchmark studies on organometallic compounds.[14] To ensure our conclusions are not affected by the choice of the computational method used in this study, we performed test calculations with different DFT methods, basis sets, and solvation models. The detailed results of these test calculations are included in the Supporting Information. These test calculations at different levels of theories give absolute activation barriers within the range of ±2−3 kcal/mol, while the relative activation barriers between the competing transition states are not affected by the choice of method.

All structures reported are the lowest energy conformers as indicated by calculations. The structures and energies of select high energy isomers and conformers are provided in the Supporting Information. We used 1,2-bis(dimethylphosphino)-benzene (DMPBz, **L1**) as a model ligand in the calculations. We have also computed the overall energy profile using the actual ligand used for this transformation (1,2-bis-(diphenylphosphino)benzene, DPPBz, **L2**) and found that the change of ligand did not affect the conclusions described here (see Supporting Information for details).

3. RESULTS AND DISCUSSION

Mechanism of the Dearomative Cyanation Cycle. We first calculated the reaction pathways for the cyanative dearomatization reaction of 2-vinylnaphthalene (**1**) and NCTS (**2**) with the borylcopper complex (**4**) to form the three possible cyanation products **8a**, **8b**, and **3c** (Catalytic Cycle I in Scheme 3). The subsequent base-catalyzed hydrogen transposition of **8a** and **8b** to furnish final products **3a** and **3b** (Catalytic Cycle II in Scheme 3) will be discussed later. The computed Gibbs free-energy profiles are shown in Figure 1. The relative enthalpies (ΔH_{sol}) are also provided in square brackets. The cyanation begins with the coordination of 2-vinylnaphthalene to the borylcopper complex (**4**) to provide π complex **5**. This step is exothermic, and the resulting π complex **5** is 6.8 kcal/mol less stable than the separate reactant **1** and **4** in terms of Gibbs free energies. Complex **5** then undergoes the facile and exergonic borocupration to afford the borylated intermediate **6** with the benzyl group η^1-bound to the copper center.[15,16] The addition of the electrophilic cyanating reagent NCTS (**2**) to the C1, C3 and benzylic positions of **6** gives rise to the formation of isomeric intermediates **7a**, **7b**, and **7c** via transition states **TS2a**, **TS2b**, and **TS2c**, respectively. **TS2a** and **TS2b** both involve a six-membered cyclic structure, where the copper center coordinates to the terminal nitrogen atom of the cyano group (Figure 1 inset and Figure 2). The cleavage of the

Scheme 3. Proposed Catalytic Cycles for the Formation of the *ortho* C−H Cyanation Product 3a

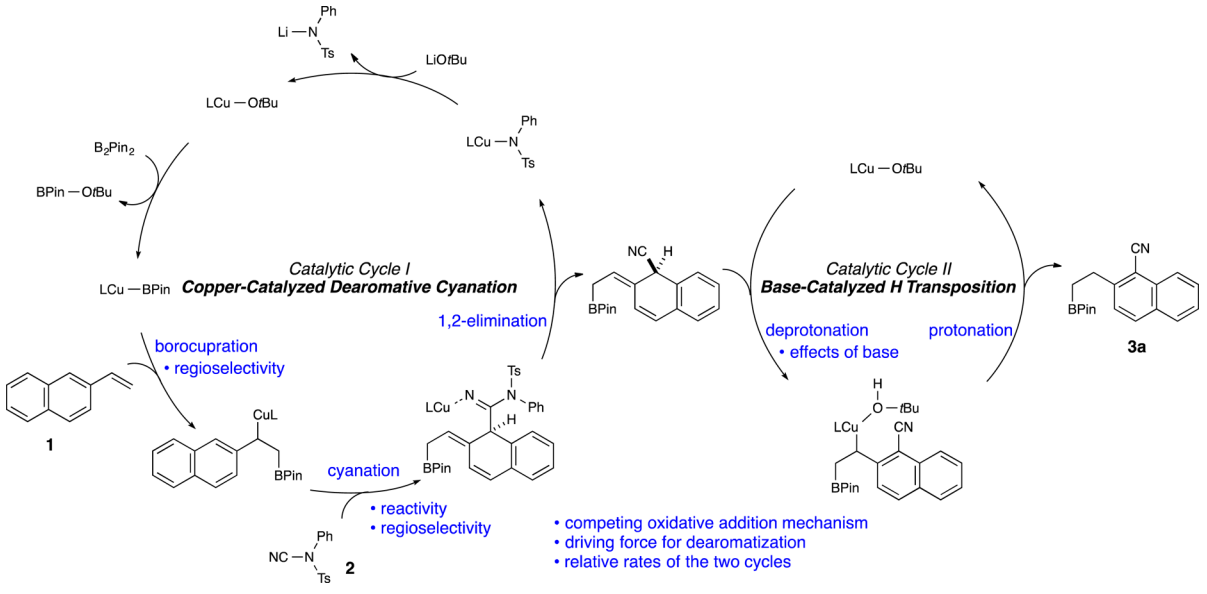

DOI: 10.1021/acscatal.5b00443
ACS Catal. 2015, 5, 2944−2951

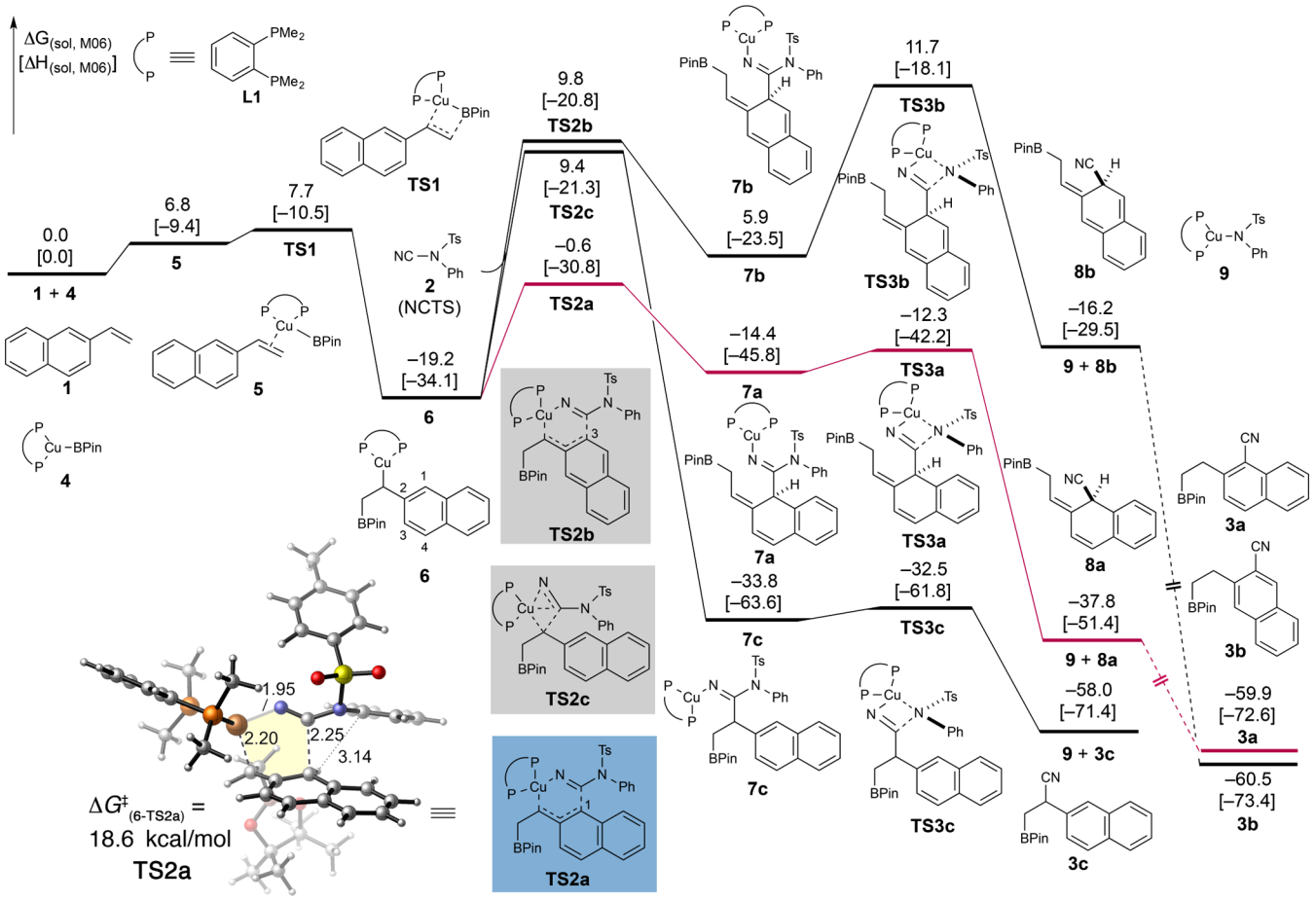

Figure 1. Computed potential energy surface of the copper-catalyzed cyanative dearomatization cycle. The major pathway for the cyanation and following steps is shown in red, and the other two regioisomeric pathways are shown in black. Gibbs free energies and enthalpies (in square brackets) are in kcal/mol. Selected bond distances in the most favorable cyanation transition state **TS2a** are labeled in Å.

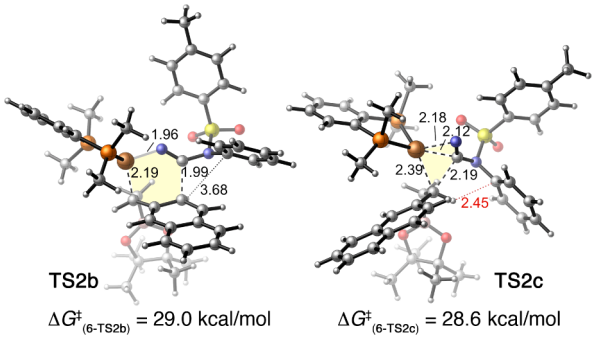

Figure 2. Optimized geometries of less favorable transition states in the electrophilic cyanation step.

Cu–C(benzylic) bond and the addition of NCTS occur in a concerted fashion. Although the aromaticity of one of the benzene rings is disrupted in the C1 attack, **TS2a** only requires an activation barrier of 18.6 kcal/mol and leads to the dearomatized intermediate **7a**, which is only 4.8 kcal/mol less stable than **6**. In contrast, owing to the loss of the aromaticity of both benzene rings, reaction at the C3 position (**TS2b**) requires an activation barrier of 10.4 kcal/mol higher than that at the C1 position and leads to a much less stable intermediate **7b**.[17] While the formation of **7c** is highly exergonic owing to the preservation of aromaticity, the benzylic cyanation involving the four-membered cyano insertion transition state **TS2c** (Figure 2) is found to be significantly less favorable than **TS2a**. The following 1,2-elimination of copper tosylamide **9** from **7a**, **7b**, and **7c** are facile, requiring low activation barriers of 2.1, 5.8, and 1.3 kcal/mol, respectively. The high exergonicity of the cyanation process (**6** + NCTS → **9** + **8a**) offers the key driving force to the irreversible formation of the dearomatized product **8a**.

Origin of Regioselectivity in Cyanative Dearomatization. The high level of regioselectivity for the dearomatized intermediate **8a** is a unique feature of the C–H cyanation reaction. To gain further understanding into the origin of the observed selectivity, we performed distortion–interaction analysis for the NCTS addition transition states **TS2a–c**.[18] The energies required to distort the benzylcopper complex **6** and NCTS into the transition state geometry ($\Delta E^{\ddagger}_{dist}$ (benzylcopper) and $\Delta E^{\ddagger}_{dist}$ (NCTS), respectively) are given in Table 1. The interaction energy between **6** and NCTS in the transition state is defined as $\Delta E^{\ddagger}_{int} = \Delta E^{\ddagger} - \Delta E^{\ddagger}_{dist}$ (benzylcopper) $- \Delta E^{\ddagger}_{dist}$ (NCTS). The preference for **TS2a** is clearly controlled by the low distortion energies of both the benzylcopper and NCTS compared to competing transition states **TS2b** and **TS2c**. The high energy required to distort the benzylcopper in **TS2b** is due to the greater extent of disrupted aromaticity. Although the aromaticity of the naphthyl ring is maintained in **TS2c** while not in **TS2a**, the distortion of benzylcopper in **TS2c** is 1.7 kcal/mol higher than that in **TS2a**. More importantly, NCTS is substantially more distorted in

DOI: 10.1021/acscatal.5b00443
ACS Catal. 2015, 5, 2944–2951

Table 1. Distortion–Interaction Analysis for the NCTS Addition Transition States TS2a–c[a]

TS	$\Delta E^{\ddagger}$	$\Delta E^{\ddagger}_{dist}$ (benzylcopper **6**)	$\Delta E^{\ddagger}_{dist}$(NCTS)	$\Delta E^{\ddagger}_{int}$
TS2a	2.7	14.1	22.4	−33.8
TS2b	13.0	21.9	27.6	−36.5
TS2c	12.1	15.8	29.6	−33.2

[a]The activation energy $\Delta E^{\ddagger}$, the distortion energy of the benzylcopper **6**, $\Delta E^{\ddagger}_{dist}$ (benzylcopper), the distortion energy of NCTS, $\Delta E^{\ddagger}_{dist}$ (NCTS), and the interaction energy $\Delta E^{\ddagger}_{int}$ are given in kcal/mol.

TS2c compared to **TS2a**. These greater distortion energies in **TS2c** are attributed to the unfavorable steric repulsions in the four-membered transition state, which, in addition, features a disfavored pentacoordinate benzylic carbon.

The different steric environments in the six-membered cyanation transition state **TS2a** and the four-membered transition state **TS2c** can be visualized in the Newman projection along the forming C–C bond shown in Figure 3.

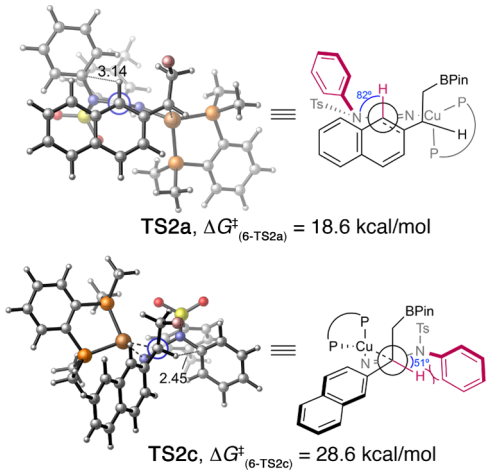

Figure 3. Newman projections of electrophilic cyanation transition states **TS2a** and **TS2c**. For clarity, the Bpin group is not shown.

In the lowest-energy conformers of **TS2a** and **TS2c**, the relatively small Ph group on NCTS is placed toward the H atom on the other reaction partner, complex **6**, to avoid steric clashes (i.e., the bulkier Ts group on NCTS is pointing away from **6**; the Ph group on NCTS is pointing away from the CH_2Bpin in **TS2c** and away from the naphthyl ring in **TS2a**). The steric interactions in the transition states mainly arise from the repulsion between the Ph and the C–H bond (shown in red in the Newman projections). In **TS2c**, insertion of the cyano group into the C(sp^3)–Cu bond results in close contact between the benzylic C–H bond and NCTS, as evidenced by the short distance (H···C = 2.45 Å) and small dihedral angle (51°) between the benzylic hydrogen atom and the phenyl group of NCTS. Such unfavorable steric interactions are not present in the cyano addition to the naphthalene's sp^2 carbon in the six-membered transition states. In **TS2a**, The corresponding N–C···C–H dihedral angle (82°) is much larger and the C···H distance (3.14 Å) is much longer than those in **TS2c**.

Additionally, NPA charge calculation of benzylcopper **6** shows that the benzylic carbon is more negatively charged than the C1 and C3 positions (Figure 4), thereby suggesting the C1 selectivity in the electrophilic cyanation is mainly controlled by substrate distortion and steric effects and not electronic effects.

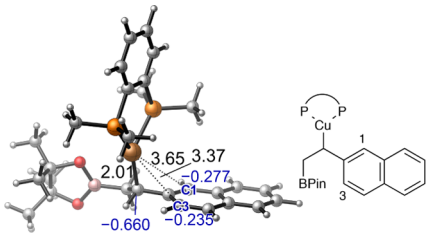

Figure 4. Optimized geometry of the benzyl copper complex **6**. The NPA charges on the benzylic carbon, C1, and C3 are shown in blue.

Regioselectivity in the Borocupration of Vinylnaphthalene. The borocupration step in the aforementioned catalytic cycle proceeds with a high level of regioselectivity in favor of the benzylcopper adduct **6**. The two possible regioisomeric pathways (via **TS1** and **TS1′**) for the borocupration step are computed and shown in Figure 5.

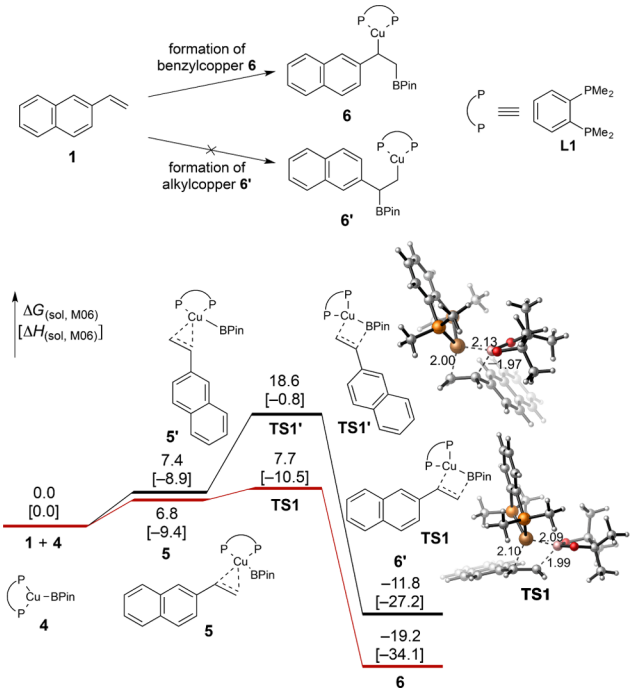

Figure 5. Free-energy profiles of possible pathways for the borocupration step to form the benzylcopper (**6**) and alkylcopper (**6′**) intermediates, respectively. The favorable pathway which leads to benzylcopper **6** is highlighted in red.

Borocupration leading to the formation of benzylcopper **6** via **TS1** is 10.9 kcal/mol more favorable than that to afford alkylcopper **6′** via **TS1′**. In addition, benzylcopper **6** is found to be 7.4 kcal/mol more stable than alkylcopper **6′**, indicating the generation of the benzylcopper species is both kinetically and thermodynamically favorable. The high regioselectivity is in line with previous computational and experimental studies[15,16] and is attributed to a combination of electronic and steric effects in the nucleophilic attack of the boryl moiety. The exclusive formation of the benzyl copper intermediate **6** is an important step that positions the Cu adjacent to the *ortho* C–H bond to facilitate the NCTS cyanation through the six-membered transition state, **TS2a**.

Oxidative Addition/Reductive Elimination Mechanism. Previous computational studies on Cu-catalyzed

DOI: 10.1021/acscatal.5b00443
ACS Catal. 2015, 5, 2944–2951

amidation, fluorination, and trifluoromethylation reactions of aryl halides supported mechanisms involving C−X oxidative addition of Cu(I) species.[19] We evaluated computationally whether a similar Cu(I)/Cu(III) redox cycle is possible in this *ortho* C−H cyanation reaction. The oxidative addition of the benzylcopper(I) complex **6** into the N−CN bond of NCTS (**2**), and the subsequent reductive elimination would directly lead to the minor product **3c**. The Gibbs free-energy profile of this pathway is shown in Figure 6a. The optimized structures of

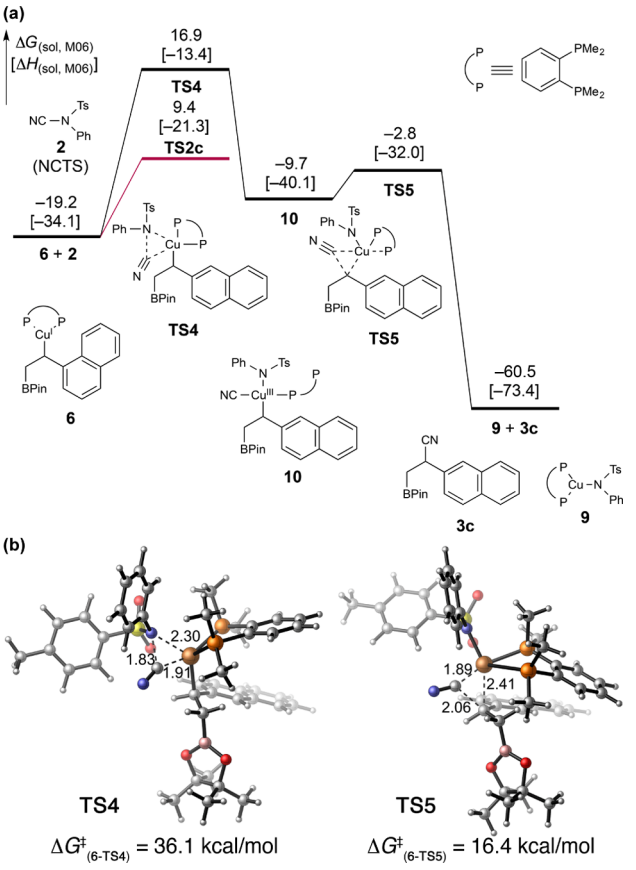

Figure 6. (a) Free-energy profile of the oxidative addition/reductive elimination mechanism involving a Cu(I)/Cu(III) redox cycle leading to the formation of benzylic cyanation product **3c**. (b) Optimized geometries of the oxidative addition (**TS4**) and reductive elimination (**TS5**) transition states.

the oxidative addition and reductive elimination transition states (**TS4** and **TS5**, respectively) are shown in Figure 6b. Oxidative addition of benzylcopper intermediate **6** to NCTS is found to be the rate-determining step and requires an activation barrier of 36.1 kcal/mol with respect to complex **6**. This is 7.5 kcal/mol higher than the barrier for cyano insertion at the benzylic position via **TS2c** and 17.5 kcal/mol higher than the most favored C1 cyanation pathway (**TS2a**). These results suggest the oxidative addition/reductive elimination mechanism is not involved in the current copper-catalyzed electrophilic cyanation.

Mechanism of the 1,3-Hydrogen Migration Cycle. The major product of the cyanation cycle, the dearomatized compound **8a**, then undergoes a formal 1,3-hydrogen migration to afford rearomatized product **3a**. We next carried out DFT calculations to investigate the mechanism of this transformation. Because the concerted thermal 1,3-H shift is a symmetry-forbidden process, we explored alternative mechanisms involving base-assisted C−H activation.[5j,20] Because both copper *tert*-butoxide (**11**) and lithium *tert*-butoxide (**13**) may be present under the reaction conditions, we considered two 1,3-hydrogen migration pathways involving these different bases. The computed free-energy profile for the reaction using **L**CuO*t*Bu as the base is shown in Figure 7. The C−H

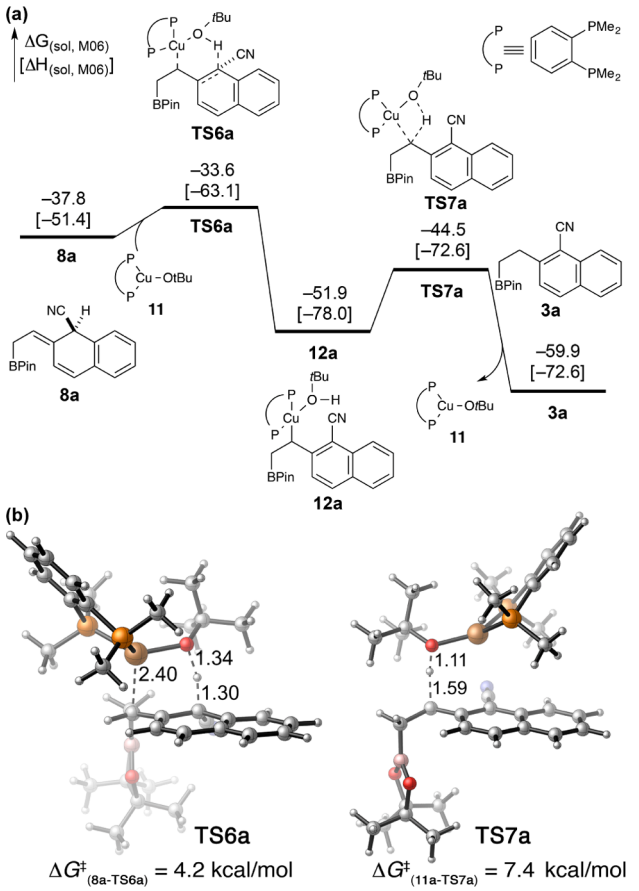

Figure 7. (a) Free-energy profile of the base-catalyzed hydrogen transposition/rearomatization using **L**CuO*t*Bu as the catalyst. (b) Optimized geometries of the C−H deprotonation (**TS6a**) and protonation (**TS7a**) transition states.

deprotonation step involves a six-membered transition state **TS6a**, where the proton is transferred to the base while the Cu−C(benzylic) bond is formed simultaneously. This base-assisted rearomatizing allylic C−H cleavage process requires a very low activation barrier of 4.2 kcal/mol, and the formation of the rearomatized complex **12a** via **TS6a** is highly exergonic. Subsequent proton transfer from the copper-bound *tert*-butanol to the benzylic carbon (**TS7a**) also requires a low activation barrier and is exergonic. Overall, the hydrogen migration cycle requires much lower activation energy than the cyanation cycle.

The 1,3-hydrogen migration pathway using LiO*t*Bu in place of **L**CuO*t*Bu occurs via a similar mechanism (Figure 8). The deprotonation with LiO*t*Bu also involves a six-membered transition state (**TS8a**), in which the proton is transferred to the base with concurrent formation of the C(benzylic)−Li bond. In the subsequent reprotonation step, the proton of the lithium-bound *tert*-butanol is transferred to the benzylic position via **TS9a**. Compared to the **L**CuO*t*Bu-catalyzed hydrogen transposition, this LiO*t*Bu-catalyzed hydrogen trans-

DOI: 10.1021/acscatal.5b00443
ACS Catal. 2015, 5, 2944−2951

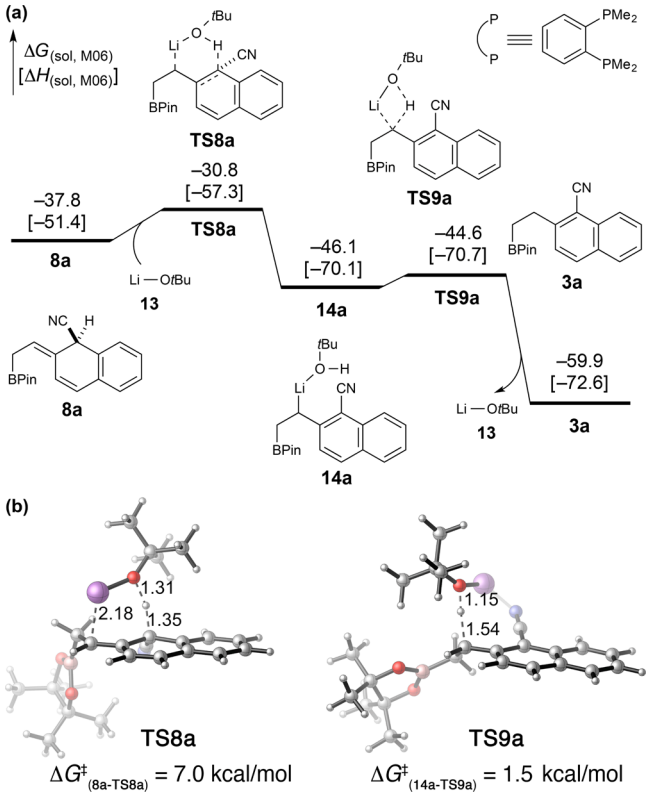

Figure 8. (a) Free-energy profile of the base-catalyzed hydrogen transposition using LiO*t*Bu as the catalyst. (b) Optimized geometries of the C−H deprotonation (**TS8a**) and protonation (**TS9a**) transition states.

position process requires a slightly higher activation barrier for the initial deprotonation step ($\Delta G^{\ddagger}$ (**8a** → **TS8a**) = 7.0 kcal/mol) but allows for the following benzylic protonation to occur with a very low activation energy ($\Delta G^{\ddagger}$ (**14a** → **TS9a**) = 1.5 kcal/mol). Overall, this LiO*t*Bu-catalyzed hydrogen transposition requires a low activation barrier of 7.0 kcal/mol, which is very close to the activation barrier using **L**CuO*t*Bu as the catalyst (7.4 kcal/mol). Taken together, these calculations demonstrate that regardless of the identity of the base catalyst, the base-catalyzed C−H activation is much faster than the electrophilic dearomative cyanation, and the cyanation step is thus the rate-determining step of the overall cascade catalysis.

Rate-Determining Step of the Overall Catalytic Cycle. Based on the computed reaction mechanisms discussed above, the most favorable pathway for the overall reaction involves five individual steps (Figures 1, 7, and 8): olefin borocupration (**TS1**) to form benzyl copper intermediate, *ortho* cyanation with NCTS (**TS2a**) and copper tosylamide elimination (**TS3a**) to form the dearomatized intermediate **8a**, and C−H deprotonation (**TS6a** or **TS8a**) and reprotonation (**TS7a** or **TS9a**). The rate-determining step is the cyanation of the benzylcopper intermediate **6** (**TS2a**), which has an activation barrier of 18.6 kcal/mol. Here, the rate-determining step precedes the C−H bond cleavage process, in line with the secondary kinetic isotope effects (KIE) observed in experiment.[4] We also calculated the KIE values for the C−H cyanation of 2-vinylnaphthalene and obtained good agreement with the experimental results (Scheme 4).[21]

Copper-Catalyzed Cyanative Dearomatization Cycle with Styrene as the Substrate. In the above calculations, we

Scheme 4. Experimental[4] and Computed Kinetic Isotope Effects in Copper-Catalyzed C(sp^2)−H Cyanation of 2-Vinylnaphthalene

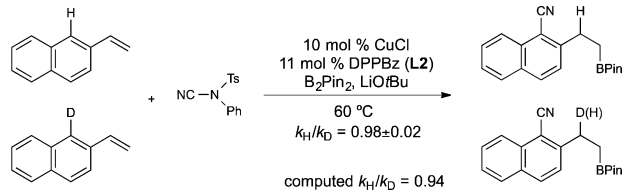

chose 2-vinylnaphthalene as the substrate to gain insight into the origin of the favorable C1 cyanation over the isomeric C3 and benzylic cyanations. Moreover, preliminary experimental studies revealed that this copper-catalyzed C−H cyanation could also be applied to simple styrene derivatives (Scheme 5).[4]

Scheme 5. Copper-Catalyzed C(sp^2)−H Cyanation of Styrene.[4]

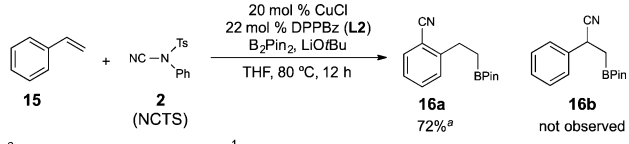

[a] Yields are determined by ^{1}H NMR spectroscopy.

To investigate the difference in reactivity between styrene and vinylnaphthalene in the cyanative dearomatization, we calculated the potential energy profiles for the *ortho* and benzylic cyanation pathways in the reaction with styrene (Figure 9).

Consistent with the experimental finding described above, calculations show that the C−H cyanation of styrene is still facile and strongly favors the *ortho* C−H cyanation product **16a** over the benzylic cyanation product **16b**. The electrophilic cyanative dearomatization (**TS11a**) remains the rate-determining step of the overall catalytic process, having an activation barrier of 23.4 kcal/mol with respect to the benzyl copper intermediate **18**. Although still feasible under the reaction conditions, this activation barrier is 4.8 kcal/mol higher than that of the C−H cyanation of 2-vinylnaphthalene ($\Delta G^{\ddagger}$ = 18.6 kcal/mol). We attribute the increased activation barrier for electrophilic dearomatization to the greater extent of aromatic stabilization of benzene as compared with naphthalene.[22] Furthermore, in accordance with the high level of regioselectivity observed experimentally (Scheme 5), calculations show that the six-membered transition state leading to the dearomatized intermediate **20a** is 5.8 kcal/mol lower in energy than the four-membered transition state resulting in the formation of benzylic cyanation product **16b**. Given the significantly fewer dearomative transformations that can be applied to nonfused simple aromatic compounds,[22] our studies could open up new avenues for the dearomatization and selective functionalization of a wide range of arene substrates.

4. CONCLUSIONS

In summary, we have performed computational studies on the mechanism and origins of selectivities in the copper-catalyzed *ortho* C−H cyanation of vinylarenes. Our DFT calculations reveal that the reaction takes place via a unique copper-catalyzed electrophilic cyanative dearomatization followed by base-catalyzed hydrogen transposition. Several factors contribute to the highly selective formation of the *ortho* cyanation

DOI: 10.1021/acscatal.5b00443
ACS Catal. 2015, 5, 2944−2951

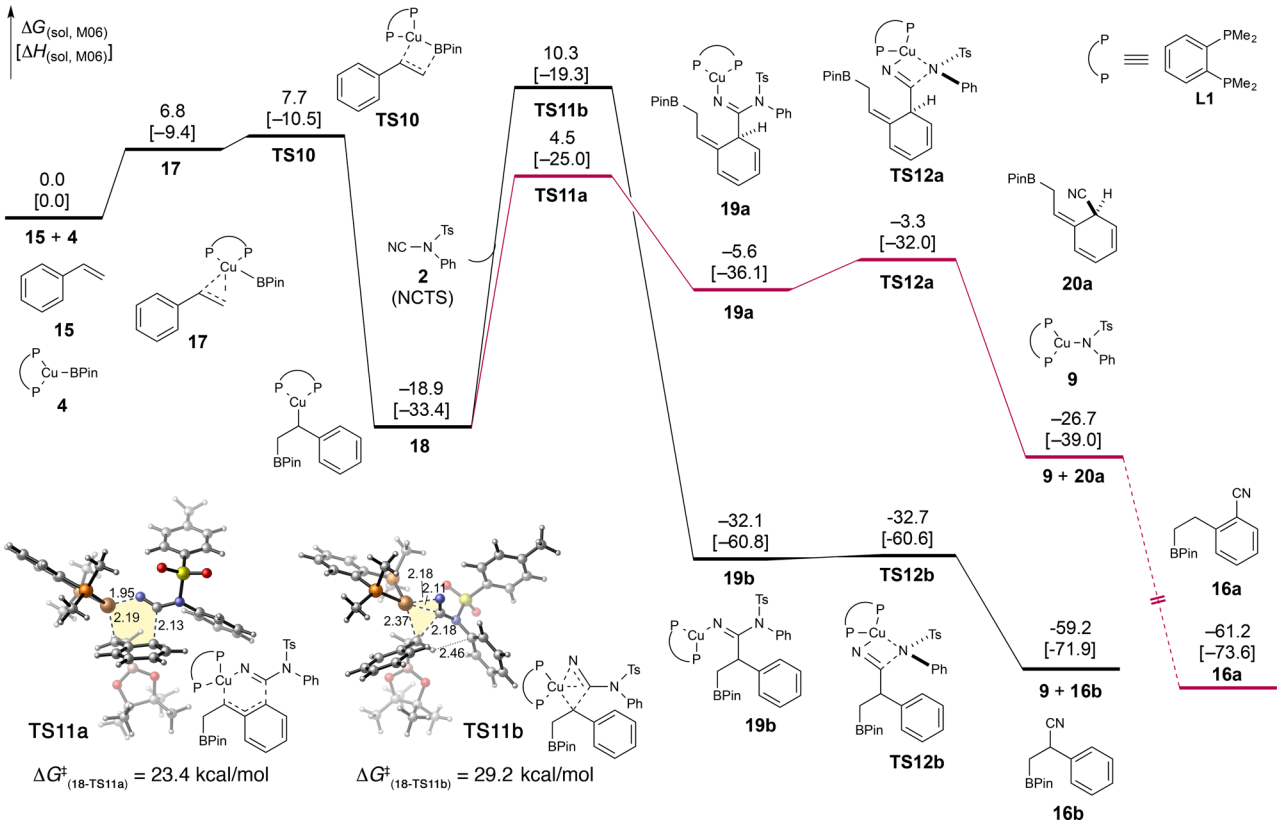

Figure 9. Computed potential energy profiles of the copper-catalyzed cyanative dearomatization cycle with styrene (**15**) as the substrate.

product via the dearomatized intermediate **8a**: (a) the *ortho* cyanation with NCTS occurs via a six-membered transition state that minimizes unfavorable steric repulsions and requires much lower barrier than the cyanation at the benzylic position; (b) the facile and highly exothermic elimination of copper tosylamide **9** after cyanation makes formation of the dearomatized intermediate **8a** irreversible; (c) intermediate **8a** is rapidly converted to the final product **3a** via base-catalyzed hydrogen transposition. Overall, the initial copper-catalyzed cyanative dearomatization cycle transforms the unactivated C(sp^2)–H bond into an allylic C–H bond that undergoes facile base-induced C–H activation to furnish the rearomatized product. We anticipate the origin of this distinct site selectivity uncovered by DFT calculations will guide the design and advancement of novel C–H functionalization reactions using the dearomatization-induced C–H activation strategy.

■ ASSOCIATED CONTENT

Supporting Information

The following file is available free of charge on the ACS Publications website at DOI: 10.1021/acscatal.5b00443.

Structures and energies of selected transition states and intermediates. Cartesian coordinates and energies of DFT-computed stationary points (PDF)

■ AUTHOR INFORMATION

Corresponding Author

*E-mail: pengliu@pitt.edu.

Notes

The authors declare no competing financial interest.

■ ACKNOWLEDGMENTS

We are grateful to Professor Stephen L. Buchwald (MIT) for support and insightful discussions. We thank the University of Pittsburgh (P.L.) and the National Institutes of Health (grant GM46059 for S.L.B.) for funding. Calculations were performed at the Center for Simulation and Modeling at the University of Pittsburgh and the Extreme Science and Engineering Discovery Environment (XSEDE) supported by NSF.

■ REFERENCES

(1) Selected recent reviews on directed C–H activation: (a) Daugulis, O.; Do, H.-Q.; Shabashov, D. *Acc. Chem. Res.* **2009**, *42*, 1074–1086. (b) Albrecht, M. *Chem. Rev.* **2010**, *110*, 576–623. (c) Colby, D. A.; Bergman, R. G.; Ellman, J. A. *Chem. Rev.* **2010**, *110*, 624–655. (d) Yeung, C. S.; Dong, V. M. *Chem. Rev.* **2011**, *111*, 1215–1292. (e) Engle, K. M.; Mei, T.-S.; Wasa, M.; Yu, J.-Q. *Acc. Chem. Res.* **2012**, *45*, 788–802. (f) Neufeldt, S. R.; Sanford, M. S. *Acc. Chem. Res.* **2012**, *45*, 936–946.

(2) Selected recent reviews on other C–H functionalizations: (a) Brückl, T.; Baxter, R. D.; Ishihara, Y.; Baran, P. S. *Acc. Chem. Res.* **2012**, *45*, 826–839. (b) Wendlandt, A. E.; Suess, A. M.; Stahl, S. S. *Angew. Chem., Int. Ed.* **2011**, *50*, 11062–11087. (c) Davies, H. M. L.; Morton, D. *Chem. Soc. Rev.* **2011**, *40*, 1857–1869. For a review on computational studies: (d) Balcells, D.; Clot, E.; Eisenstein, O. *Chem. Rev.* **2010**, *110*, 749–823.

(3) (a) Tobisu, M.; Hyodo, I.; Onoe, M.; Chatani, N. *Chem. Commun.* **2008**, 6013–6015. (b) Gandeepan, P.; Cheng, C.-H. *J. Am. Chem. Soc.* **2012**, *134*, 5738–5741.

(4) Yang, Y.; Buchwald, S. L. *Angew. Chem., Int. Ed.* **2014**, *53*, 8677–8681.

(5) Recent examples of copper-mediated/catalyzed C–H activation: (a) Phipps, R. J.; Grimster, N. P.; Gaunt, M. J. *J. Am. Chem. Soc.* **2008**, *130*, 8172–8174. (b) Phipps, R. J.; Gaunt, M. J. *Science* **2009**, *323*, 1593–1597. (c) Tran, L. D.; Popov, I.; Daugulis, O. *J. Am. Chem. Soc.*

DOI: 10.1021/acscatal.5b00443
ACS Catal. 2015, 5, 2944–2951

2012, *134*, 18237−18240. (d) Truong, T.; Klimovica, K.; Daugulis, O. *J. Am. Chem. Soc.* **2013**, *135*, 9342−9345. (e) Nishino, M.; Hirano, K.; Satoh, T.; Miura, M. *Angew. Chem., Int. Ed.* **2013**, *52*, 4457−4461. (f) Shang, M.; Sun, S.-Z.; Dai, H.-X.; Yu, J.-Q. *J. Am. Chem. Soc.* **2014**, *136*, 3354−3357. (g) Shang, M.; Wang, H.-L.; Sun, S.-Z.; Dai, H.-X.; Yu, J.-Q. *J. Am. Chem. Soc.* **2014**, *136*, 11590−11593. For computational and mechanistic studies: (h) Badiei, Y. M.; Dinescu, A.; Dai, X.; Palomino, R. M.; Heinemann, F. W.; Cundari, T. R.; Warren, T. H. *Angew. Chem., Int. Ed.* **2008**, *47*, 9961−9964. (i) Chen, B.; Hou, X.-L.; Li, Y.-X.; Wu, Y.-D. *J. Am. Chem. Soc.* **2011**, *133*, 7668−7671. (j) Wang, M.; Fan, T.; Lin, Z. *Organometallics* **2012**, *31*, 560−569. (k) Suess, A. M.; Ertem, M. Z.; Cramer, C. J.; Stahl, S. S. *J. Am. Chem. Soc.* **2013**, *135*, 9797−9804.

(6) For applications of NCTS (N-cyano-N-phenyl-p-toluenesulfonamide) in electrophilic cyanations: (a) Anbarasan, P.; Neumann, H.; Beller, M. *Angew. Chem., Int. Ed.* **2011**, *50*, 519−522. (b) Anbarasan, P.; Neumann, H.; Beller, M. *Chem. - Eur. J.* **2011**, *17*, 4217−4222. (c) Yang, Y.; Zhang, Y.; Wang, J. *Org. Lett.* **2011**, *13*, 5608−5611. (d) Gong, T.-J.; Xiao, B.; Cheng, W.-M.; Su, W.; Xu, J.; Liu, Z.-J.; Liu, L.; Fu, Y. *J. Am. Chem. Soc.* **2013**, *135*, 10630−10633. (e) Liu, W.; Ackermann, L. *Chem. Commun.* **2014**, *50*, 1878−1881. (f) Yu, D.-G.; Gensch, T.; de Azambuja, F.; Vasquez-Cespedes, S.; Glorius, F. *J. Am. Chem. Soc.* **2014**, *136*, 17722−17725. (g) Li, J.; Ackermann, L. *Angew. Chem., Int. Ed.* **2015**, *54*, 3635−3638.

(7) For a recent review on benzylmetal complexes and related dearomatizaton reactions: (a) Trost, B. M.; Czabaniuk, L. C. *Angew. Chem., Int. Ed.* **2014**, *53*, 2826−2851. For computational studies: (b) Ariafard, A.; Lin, Z. *J. Am. Chem. Soc.* **2006**, *128*, 13010−13016. (c) Xie, H.; Zhang, H.; Lin, Z. *Organometallics* **2013**, *32*, 2336−2343. (d) Hoveln, R. V.; Hudson, B. M.; Wedler, H. B.; Bates, D. M.; Le Gros, G.; Tantillo, D. J.; Schomaker, J. M. *J. Am. Chem. Soc.* **2015**, DOI: 10.1021/ja511236d.

(8) Frisch, M. J.; Trucks, G. W.; Schlegel, H. B.; Scuseria, G. E.; Robb, M. A.; Cheeseman, J. R.; Scalmani, G.; Barone, V.; Mennucci, B.; Petersson, G. A.; Nakatsuji, H.; Caricato, M.; Li, X.; Hratchian, H. P.; Izmaylov, A. F.; Bloino, J.; Zheng, G.; Sonnenberg, J. L.; Hada, M.; Ehara, M.; Toyota, K.; Fukuda, R.; Hasegawa, J.; Ishida, M.; Nakajima, T.; Honda, Y.; Kitao, O.; Nakai, H.; Vreven, T.; Montgomery, J. A., Jr.; Peralta, J. E.; Ogliaro, F.; Bearpark, M.; Heyd, J. J.; Brothers, E.; Kudin, K. N.; Staroverov, V. N.; Kobayashi, R.; Normand, J.; Raghavachari, K.; Rendell, A.; Burant, J. C.; Iyengar, S. S.; Tomasi, J.; Cossi, M.; Rega, N.; Millam, J. M.; Klene, M.; Knox, J. E.; Cross, J. B.; Bakken, V.; Adamo, C.; Jaramillo, J.; Gomperts, R.; Stratmann, R. E.; Yazyev, O.; Austin, A. J.; Cammi, R.; Pomelli, C.; Ochterski, J. W.; Martin, R. L.; Morokuma, K.; Zakrzewski, V. G.; Voth, G. A.; Salvador, P.; Dannenberg, J. J.; Dapprich, S.; Daniels, A. D.; Farkas, Ö.; Foresman, J. B.; Ortiz, J. V.; Cioslowski, J.; Fox, D. J. *Gaussian 09*, , revision D.01; Gaussian, Inc.: Wallingford, CT, 2010.

(9) *CYLview*, 1.0b; Legault, C. Y. Université de Sherbrooke: Quebec, Canada, 2009; http://www.cylview.org.

(10) (a) Becke, A. D. *J. Chem. Phys.* **1993**, *98*, 5648−5652. (b) Lee, C.; Yang, W.; Parr, R. G. *Phys. Rev. B: Condens. Matter Mater. Phys.* **1988**, *37*, 785−789.

(11) (a) Zhao, Y.; Truhlar, D. G. *Theor. Chem. Acc.* **2008**, *120*, 215−241. (b) Zhao, Y.; Truhlar, D. G. *Acc. Chem. Res.* **2008**, *41*, 157−167.

(12) Marenich, A. V.; Cramer, C. J.; Truhlar, D. G. *J. Phys. Chem. B* **2009**, *113*, 6378−6396.

(13) For examples of our recent computational studies employing B3LYP in geometry optimization and M06 in single point energy calculations for organometallic compounds: (a) Cannon, J. S.; Zou, L.; Liu, P.; Lan, Y.; O'Leary, D. J.; Houk, K. N.; Grubbs, R. H. *J. Am. Chem. Soc.* **2014**, *136*, 6733−6743. (b) Green, A. G.; Liu, P.; Merlic, C. A.; Houk, K. N. *J. Am. Chem. Soc.* **2014**, *136*, 4575−4583. (c) Cheng, G.-J.; Yang, Y.-F.; Liu, P.; Chen, P.; Sun, T.-Y.; Li, G.; Zhang, X.; Houk, K. N.; Yu, J.-Q.; Wu, Y.-D. *J. Am. Chem. Soc.* **2014**, *136*, 894−897. (d) Yang, Y.-F.; Cheng, G.-J.; Liu, P.; Leow, D.; Sun, T.-Y.; Chen, P.; Zhang, X.; Yu, J.-Q.; Wu, Y.-D.; Houk, K. N. *J. Am. Chem. Soc.* **2014**, *136*, 344−355.

(14) (a) Simon, L.; Goodman, J. M. *Org. Biomol. Chem.* **2011**, *9*, 689−700. (b) Poater, A.; Pump, E.; Vummaleti, S. V. C.; Cavallo, L. *J. Chem. Theory Comput.* **2014**, *10*, 4442−4448.

(15) (a) Dang, L.; Zhao, H.; Lin, Z.; Marder, T. B. *Organometallics* **2007**, *26*, 2824−2832. (b) Zhao, H.; Lin, Z.; Marder, T. B. *J. Am. Chem. Soc.* **2006**, *128*, 15637−15643.

(16) For experimental studies on styrene borocupration: (a) Laitar, D. S.; Tsui, E. Y.; Sadighi, J. P. *Organometallics* **2006**, *25*, 2405−2408. (b) Lillo, V.; Fructos, M. R.; Ramírez, J.; Braga, A. A. C.; Maseras, F.; Díaz-Requejo, M. M.; Pérez, P. J.; Fernández, E. *Chem. - Eur. J.* **2007**, *13*, 2614−2621. (c) Lee, Y.; Hoveyda, A. H. *J. Am. Chem. Soc.* **2009**, *131*, 3160−3161. (d) Zhong, C.; Kunii, S.; Kosaka, Y.; Sawamura, M.; Ito, H. *J. Am. Chem. Soc.* **2010**, *132*, 11440−11442. (e) Ito, H.; Toyoda, T.; Sawamura, M. *J. Am. Chem. Soc.* **2010**, *132*, 5990−5992. (f) Corberán, R.; Mszar, N. W.; Hoveyda, A. H. *Angew. Chem., Int. Ed.* **2011**, *50*, 7079−7082. (g) Matsuda, N.; Hirano, K.; Satoh, T.; Miura, M. *J. Am. Chem. Soc.* **2013**, *135*, 4934−4937. (h) Smith, K. B.; Logan, K. M.; You, W.; Brown, M. K. *Chem. - Eur. J.* **2014**, *20*, 12032−12036.

(17) For transition-metal-catalyzed regioselective C−H arylation of naphthalenes: (a) Hickman, A. J.; Sanford, M. S. *ACS Catal.* **2011**, *1*, 170−174. (b) Wagner, A. M.; Hickman, A. J.; Sanford, M. S. *J. Am. Chem. Soc.* **2013**, *135*, 15710−15713.

(18) (a) Ess, D. H.; Houk, K. N. *J. Am. Chem. Soc.* **2007**, *129*, 10646−10647. (b) van Zeist, W.-J.; Bickelhaupt, F. M. *Org. Biomol. Chem.* **2010**, *8*, 3118−3127.

(19) For computational studies involving the oxidative addition of Cu(I) to aryl halides: (a) Zhang, S. L.; Liu, L.; Fu, Y.; Guo, Q. X. *Organometallics* **2007**, *26*, 4546−4554. (b) Tye, J. W.; Weng, Z.; Johns, A. M.; Incarvito, C. D.; Hartwig, J. F. *J. Am. Chem. Soc.* **2008**, *130*, 9971−9983. (c) Ichiishi, N.; Canty, A. J.; Yates, B. F.; Sanford, M. S. *Organometallics* **2014**, *33*, 5525−5534. (d) Konovalov, A. I.; Lishchynskyi, A.; Grushin, V. V. *J. Am. Chem. Soc.* **2014**, *136*, 13410−13425.

(20) Engelin, C.; Jensen, T.; Rodriguez-Rodriguez, S.; Fristrup, P. *ACS Catal.* **2013**, *3*, 294−302.

(21) The KIEs were calculated from the overall activation Gibbs free energies (**6** + **2** → **TS2a**) with the deuterated and nondeuterated substrates at 60 °C. To ensure the accuracy of the computed low frequencies, tighter geometry and SCF convergence criteria ("opt = vtight scf = (conver = 10)") and the "ultrafine" integration grid in Gaussian 09 were used in the B3LYP geometry optimizations and vibrational frequency calculations. A scaling factor of 0.96 was used for the B3LYP-calculated frequencies. A mixed basis set of SDD for Cu and 6-31G(d) for other atoms were used in the KIE calculations, which is the same level of theory used for geometry optimizations in this study.

(22) (a) Pape, A. R.; Kaliappan, K. P.; Kundig, E. P. *Chem. Rev.* **2000**, *100*, 2917−2940. (b) Roche, S. P.; Porco, J. A., Jr. *Angew. Chem., Int. Ed.* **2011**, *50*, 4068−4093. (c) Zhuo, C.-X.; Zheng, C.; You, S.-L. *Acc. Chem. Res.* **2014**, *47*, 2558−2573.

DOI: 10.1021/acscatal.5b00443
ACS Catal. 2015, 5, 2944−2951